JOURNAL OF SPACECRAFT AND ROCKETS
Vol. 33, No. 3, May–June 1996

Aeroprediction Code for Angles of Attack Above 30 Degrees

F. G. Moore,* R. M. McInville,† and T. Hymer†
U.S. Naval Surface Warfare Center, Dahlgren, Virginia 22448-5100

The U.S. Naval Surface Warfare Center Dahlgren Division aeroprediction code has been extended to angles of attack greater than 30 deg. To accomplish this, several databases were used to approximate the nonlinearities in individual missile component aerodynamics. Theoretical aerodynamic methods were used at small angles of attack. The new semiempirical model was then applied to several configurations and the empirical constants fine tuned so as to minimize some of the errors associated with wind-tunnel measurements of component aerodynamics at high angles of attack. New and improved technology developed includes 1) extension of the wing-body and body-wing interference factor methodology above angle of attack of 30 deg for both zero and nonzero control deflections and 2) refinements in body-alone normal force and center-of-pressure prediction to account for Reynolds number, and transonic and asymmetrically shed body vortices. All methodology is developed for the Φ = 0-deg (or fins in plus) roll orientation. Comparison of the new methodology to several cases outside the databases on which the methodology was developed appears to indicate the average accuracy goals of $\pm 10\%$ on normal force and $\pm 4\%$ of body length on center of pressure were maintained for the higher angles of attack.

Nomenclature

A_P = planform area of the body or wing in the crossflow plane, ft^2
A_{ref} = reference area (maximum cross-sectional area of body, if a body is present, or planform area of wing, if wing alone), ft^2
A_W, S_W = planform area of wing in crossflow plane, ft^2
A_{wetted} = area of body or wing that flow touches
a_0, a_1, a_2, a_3, a_4 = constants used in nonlinear wing-alone model
b = wing span (not including body), ft
C_A = axial force coefficient
$C_{A_B}, C_{A_F}, C_{A_W}$ = base, skin-friction, and wave components, respectively, of axial force coefficient
C_{D_C} = crossflow drag coefficient
C_{F_ℓ}, C_{F_T} = laminar and turbulent skin friction coefficients, respectively
C_M = pitching moment coefficient (based on reference area and body diameter, if body present, or mean aerodynamic chord, if wing alone)
C_N = normal force coefficient
C_{N_B} = normal force coefficient of body alone
C_{N_L} = linear component of normal force coefficient
$C_{N_{NL}}$ = nonlinear component of normal force coefficient
$C_{N_{T(V)}}$ = negative normal force coefficient component on tail due to wing or canard-shed vortex
C_{N_W} = normal force coefficient of wing alone
C_{N_α} = normal force coefficient derivative
d = body diameter, ft
$dK_{W(B)}/d\alpha$, $dK_{B(W)}/d\alpha$ = rate at which $K_{W(B)}$ or $K_{B(W)}$ decreases
F, C_1, C_2, C_3 = dimensionless empirical factors used in nonlinear models of $k_{W(B)}$ and $C_{N_{T(V)}}$ to approximate effects resulting from high angle of attack or control deflection
f_W, f_T = lateral location of wing or tail vortex (measured in feet from body centerline)
i = tail interference factor
$K_{B(W)}, K_{B(T)}$ = ratio of additional body normal force coefficient in presence of wing, or tail to wing, or tail alone normal force coefficient at $\delta = 0$ deg
$K_{W(B)}, K_{T(B)}$ = ratio of normal force coefficient of wing or tail in presence of body to that of wing or tail alone at $\delta = 0$ deg
$k_{B(W)}, k_{B(T)}$ = ratio of additional body normal force coefficient resulting from presence of wing or tail at a control deflection to that of wing or tail alone at $\alpha = 0$ deg
$k_{W(B)}, k_{T(B)}$ = ratio of wing or tail normal force coefficient in presence of body resulting from a control deflection to that of wing or tail alone at $\alpha = 0$ deg
$[K_{B(W)}]_{\min}$ = minimum value of $K_{B(W)}$ as percent of slender-body or linear theory value
ℓ = body length, ft
M = Mach number
M_C = normal Mach number to body axis, $M \sin\alpha$
Re_{crit} = critical Reynolds number where flow transitions from separating on the forward part of a circular cylinder to the rear part
Re_X = Reynolds number based on point where boundary-layer transition occurs
r = radius of body, ft
s = wing or tail semispan plus the body radius in wing–body lift methodology
X_{CP} = center of pressure, feet or calibers, from some reference point that can be specified
$(X_{CP})_L$, $(X_{CP})_{NL}$ = center of pressure of linear and nonlinear terms of normal force
α = angle of attack, deg
α_C = angle of attack where wing–body interference factor starts decreasing from its slender-body theory value, deg
α_D = angle of attack where the wing–body interference factor reaches a minimum, deg
α_M = angle of attack where $K_{W(B)}$ reaches its limiting value
α_W, α_T = local angle of attack of wing or tail, $\alpha + \delta_w$ or $\alpha + \delta_T$, respectively, deg
α_1, α_2 = angles of attack used in nonlinear model for $K_{B(W)}$
$[\Delta K_{W(B)}]_{\alpha=0}$, $[\Delta K_{B(W)}]_{\alpha=0}$ = amount that the experimental values of $K_{W(B)}$ and $K_{B(W)}$ exceed slender body theory at $\alpha = 0$ deg

Received April 27, 1995; revision received Oct. 23, 1995; accepted for publication Dec. 15, 1995.

*Senior Aerodynamicist, Weapons Systems Department, Dahlgren Division. Associate Fellow AIAA.
†Aerospace Engineer, Aeromechanics Branch, Weapon Systems Department, Dahlgren Division.

δ = control deflection, deg
δ_W, δ_T = deflection of wing or tail surfaces, positive leading edge up, deg
η = parameter used in viscous crossflow theory for nonlinear body normal force (in this context, it is the normal force of a circular cylinder of given length-to-diameter ratio to that of a cylinder of infinite length)
λ = taper ratio of a lifting surface, c_t/c_r
Φ = circumferential position around body where $\Phi = 0$ is leeward plane, (deg) and fins are in plus (+) fin orientation
∞ = freestream conditions

Introduction

ESTIMATING missile aerothermodynamics over the flight regime where missiles fly is quite important in all phases of design. These aerodynamics are used by the flight dynamicist to estimate range performance and miss distance, the heating information is used to perform heat-transfer analysis, and the aerodynamic and thermodynamic loads are used by the structural engineer to estimate structural integrity of the configuration. Missiles that are launched from a vertical launcher can experience angles of attack (AOA) approaching 90 deg if a strong crosswind is present. Missiles that are launched from aircraft undergoing maneuvers can also experience AOA approaching 60 deg. Finally, terminally guided missiles undergoing maneuvers in the endgame can anticipate AOA as high as 40 deg. Hence, it is necessary to have aerodynamics estimates above 30-deg AOA to cover the flight regime for all possible conditions.

The recent version of the Naval Surface Warfare Center, Dahlgren Division, Aeroprediction Code (APC) released to the public in 1993 and referred to as AP93[1] was limited to AOA of about 30 deg because the wing-alone, wing–body, and body–wing interference aerodynamics were developed only to about 30-deg AOA. In some cases, the accuracy degraded at an AOA of 25 deg. The wing-alone methodology was recently extended by Moore and McInville[2] to AOA of 180 deg by developing a new fourth-order method vs a second-order technique used in the AP93. The fourth-order method gives improved accuracy over the second-order technique in the AOA range 0–30 deg, in addition to extending the AOA range to 180 deg (Ref. 2).

This paper develops the complementary extension of the body-alone and interference factor methodology above AOA of 30 deg. This new technology, along with that in the Moore and McInville study,[2] will allow the AP93 code to be extended in AOA capability so the operational AOA boundary for missile flight can be covered. This new version of the code will be called AP95.

Although the extension to higher AOA represents a significant step forward in modeling nonlinearities in an engineering version of an aeroprediction code, there are still several nonlinearities not modeled or modeled only approximately in AP95. These include roll-dependent or cross-coupling aerodynamics effects; asymmetric body-shed vortices, which occur for Mach numbers less than 2 and AOA between about 20 and 60 deg; and internal shock interactions from the nose to the tail or wing, or from the wing to the tail. The latter effects typically occur above AOA of about 30 deg and at supersonic or hypersonic Mach numbers. These phenomena will be discussed more fully in the analysis section. This paper will only summarize the new methods and present a few results. For details, the reader is referred to Ref. 3.

Analysis

Discussion of Nonlinear Missile Aerodynamics

The physical phenomena involved in missile aerodynamics should be examined before proceeding with the development of nonlinear methods for high AOA. Figure 1 attempts to describe missile aerodynamics in a generic way as a function of the AOA and Mach number regions desired from an operational standpoint. At low AOA, the aerodynamics are mostly linear (except for transonic flow), and linearized and slender-body aerodynamic methods prove very effective in providing acceptable accuracy for approximate aerodynamic prediction codes.[4] As AOA increases above 10 deg, the nonlinearities associated with AOA become increasingly important at all Mach numbers, and the nonlinear compressibility effects become important above $M_\infty \approx 0.6$. Linearized codes can still be used in the range 10 deg $< \alpha <$ 20 deg, but with degraded accuracy. As AOA increases above 20 deg, the flow becomes strongly nonlinear but still reasonably well behaved in terms of static aerodynamics as a function of AOA. At these AOA, nonlinear aerodynamic methods are required for reasonable accuracy. For approximate aerodynamic codes, these nonlinear methods are typically empirical or semiempirical.[1,5,6]

Above AOA of about 25 deg and below M_∞ of about 2, another nonlinear phenomenon occurs on many configurations because of the asymmetric shedding of body vortices. This phenomenon is the strongest in the subsonic Mach number range and starts to dissipate at crossflow Mach numbers of about 0.5 (Ref. 7). Although the phenomenon is reasonably well understood, it is predictable in the general sense only in terms of upper bounds on side forces created by the shedding. Forward-placed fins or control surfaces tend to minimize the effect.

Above AOA of about 30 deg and $M_\infty \approx 2.0$, strong shock interactions can cause very strong effects on the aerodynamics. These effects exhibit themselves in the form of loss of static stability and normal force. Typical shocks of interest are the bow shock intersecting a control surface or a forward lifting surface shock intersecting a tail surface. The latter problem appears to be more critical since the moment arm to the tail is generally longer than to the wing or canard. Aerodynamics in this region may not be well behaved in terms of either monotonically increasing or decreasing.

The question arises as to whether the databases that will be used to estimate the nonlinear aerodynamic phenomena will provide acceptable results. For a body-alone configuration at low Mach numbers, the normal force will vary somewhat because of the presence of the side force, but basically can be estimated with reasonable accuracy if boundary-layer transition in the crossflow plane is predicted accurately. For Mach numbers approaching 2 and greater, past attempts have shown the methods used in AP93 to be directly applicable at higher AOA with few changes.[1] However, these methods were based on empirical approximations to the nonlinearities occurring to the wing, body, and wing–body interference based on a component buildup database.[8,9] This database had various size wings with a single body. Hence, no wing–tail shock interactions or wing–tail interference could be estimated directly.

In summary, it is anticipated that all of the nonlinearities in missile aerodynamics except the internal shock interaction of the wing and tail and wing–tail interference can be approximately accounted for using the available databases. The body side force at low Mach number will not be approximated since only in-plane aerodynamics

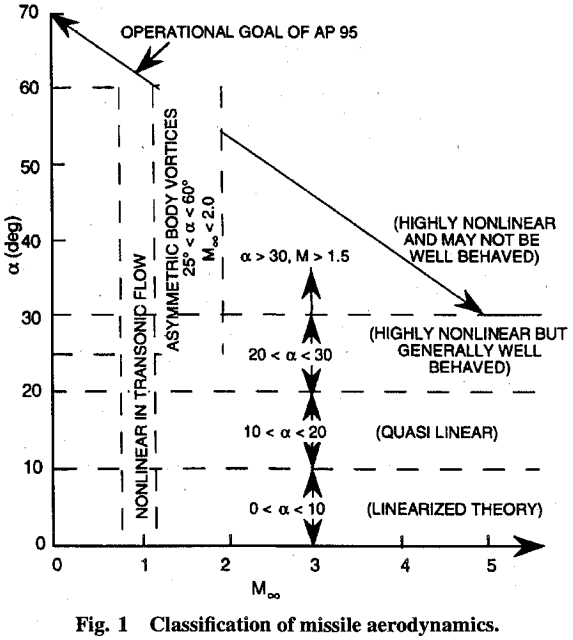

Fig. 1 Classification of missile aerodynamics.

($\Phi = 0$) are being considered. The high-AOA canard or wing-shed vortex and control-deflection effects can be approximately modeled with empirical experiments compared to other databases.[1] Note at the outset, however, that by extending the flow computations into the highly nonlinear, may-not-be-well-behaved region of Fig. 1, the accuracy available in the AP93 for the $\alpha \leq 30$-deg cases may be somewhat degraded. On average, these accuracy levels were $\pm 10\%$ on axial force coefficient and normal force coefficient and $\pm 4\%$ length for center of pressure. There were cases where these accuracy bounds were exceeded at a given α and M. However, when all α and M cases were averaged for a given configuration, these accuracy bounds were found to hold for the cases considered to date. Although the stated average accuracy goal will be difficult to maintain for AOA > 30 deg, it will still be the goal of this effort.

Approach to Develop Nonlinear Aeroprediction Code

The overall analysis approach to the development of a nonlinear high-AOA APC is as follows: 1) Use linear theory/slender-body theory (SBT)/second-order methods primarily for low AOA ($\alpha \leq 10$ deg). 2) Use missile component databases to develop empirical estimates of component aerodynamics at high AOA. 3) Develop mathematical models for these empirical, high-AOA methods when feasible. 4) Apply the methods to overall missile configurations outside the database and adjust the parameters in the mathematical model to try to minimize errors in the databases.

Since the small AOA aerodynamic methods for computing axial force work well and are well documented,[1,4] the emphasis in this paper will be on the new nonlinear methods for computing high-AOA normal force and center of pressure. The total normal force equation[10] for a wing–body–tail configuration at a given AOA, control deflection, and Mach number is

$$C_N = C_{N_B} + \left[\left(K_{W(B)} + K_{B(W)}\right)\alpha + \left(k_{W(B)} + k_{B(W)}\right)\delta_W\right]\left(C_{N_\alpha}\right)_W + \left[\left(K_{T(B)} + K_{B(T)}\right)\alpha + \left(k_{T(B)} + k_{B(T)}\right)\delta_T\right]\left(C_{N_\alpha}\right)_T + C_{N_{T(V)}} \tag{1}$$

The first term in Eq. (1) is the normal force of the body alone including the linear and nonlinear components; the second term is the contribution of the wing (or canard) including interference effects and control deflection; the third term is the contribution of the tail including interference effects and control deflection; the last term is the negative downwash effect on the tail resulting from wing-shed or body-shed vortices. K represents the interference of the configuration with respect to AOA, and k represents the interference with respect to control deflection. Subscripts $W(B)$ and $T(B)$ represent the change (or interference effect) of the wing and tail in the presence of the body, whereas subscripts $B(W)$ and $B(T)$ indicate the additional lift (or interference effect) on the body because of the presence of wings or tails.

When Eq. (1) was originally defined, it was associated with the linear aerodynamics only.[10] However, the approach of the present work is to define nonlinearities of each of the terms in Eq. (1) using empirical or semiempirical methods. These nonlinear terms are then added to their linear counterparts, which are predicted analytically. Each of the terms in Eq. (1) will be discussed in terms of improvements made.

Body-Alone Improvements

The primary focus in the body-alone work has been an attempt to improve the modeling of the nonlinear normal force at crossflow Mach numbers below 0.6, to include compressibility effects in the laminar skin-friction drag computation, and to improve upon the center of pressure caused by the nonlinear aerodynamics. Each of these improvements will be briefly discussed. For details, the reader is once again referred to Ref. 3.

The nonlinear contribution to the normal force is generally expressed as

$$C_{N_{NL}} = \eta C_{D_C} A_P / A_{\text{ref}} \sin^2 \alpha \tag{2}$$

As explained in detail,[7,11] C_{D_C} varies in a complex fashion for $M_C < 0.5$. Below a certain critical Reynolds number (Re_{crit}), the body boundary layer is laminar, and the flow separates at about the 90–100 deg circumferential location (where $\Phi = 0$ deg is the leeward plane), producing a large wake region and a relatively constant value of C_{D_C}. At Re_{crit}, the separated boundary layer transitions to turbulent and reattaches, remaining attached until approximately the 40-deg circumferential location (140 deg from the windward plane). The resulting smaller wake produces a sudden decrease in the value of C_{D_C}. As the Reynolds number increases further, transition moves forward and the laminar separation bubble disappears, leading to an eventual stabilization of C_{D_C} as the turbulent separation becomes fixed at about the 80-deg location. At crossflow Mach numbers greater than 0.5, localized supersonic regions develop as the flow expands around the body. The shocks that are produced by these supersonic pockets are strong enough to separate the boundary layer regardless of its laminar or turbulent state, and the drag bucket disappears, leaving C_{D_C} virtually independent of the state of the boundary layer.

As pointed out in Ref. 7, the observed value of Re_{crit} can vary drastically from test to test and from one wind tunnel to another because of a number of factors including tunnel turbulence, wall and model roughness, and model vibration. In fact, over an order-of-magnitude difference has been found using the same model in different wind tunnels.

The C_{D_C} model that has been incorporated into AP95 was developed primarily using the data from Refs. 8 and 11. The Ref. 8 body-alone data were obtained using a model with a 3.0-caliber tangent ogive nose and an overall length of 12.33 calibers. Body diameter was 3.0 in. The Ref. 11 data represent measurements on two configurations. One has a 2.5-caliber ogive nose and a total length of 9.5 calibers. The other has a 3.5-caliber ogive nose and a total length of 10.5 calibers. The body diameter in both cases is 1.5 in. Freestream Mach numbers ranged from 0.6 to 1.2, and AOA varied from 5 deg up to 60 deg. Since only total C_N values were given, C_{D_C} was extracted first by subtracting the linear component as determined by slender-body theory, for simplicity. Equation (2) was then used to compute C_{D_C}, with the value of η coming from Jorgenson.[11]

Because of the variation of transition-linked phenomena with test conditions, Re_{crit} can be adjusted in the AP95 input file. Its default value is the theoretical two-dimensional cylinder result of 330,000. In addition, the location of the drag bucket can be shifted horizontally by specifying a second input parameter.

The body-alone center of pressure is determined by summing the separately determined linear and nonlinear contributions to the total moment and then dividing by the combined normal force, i.e.,

$$X_{CP} = \frac{C_{N_L}(X_{CP})_L + C_{N_{NL}}(X_{CP})_{NL}}{C_{N_L} + C_{N_{NL}}} \tag{3}$$

The second modification in the body-alone methodology of the AP93 is in the center-of-pressure change with AOA. Two nonlinear phenomena are present that Eq. (3) does not fully account for. One phenomenon is the shift in center of pressure, which occurs as a result of the asymmetric body vortices, which typically occur above AOA = 25 deg and below $M_\infty = 2.0$. This phenomenon appears to affect the normal force only slightly but shifts the center of pressure forward. The second phenomenon occurs in the transonic flow range where a shock forms on the body as the flow approaches sonic conditions. The center-of-pressure shift tends to be forward from this phenomenon as well.

To estimate the center-of-pressure shifts, two different databases[8,12] were used and were nondimensionalized with respect to body length. In implementing these results into complete missile configurations, the shifts in the transonic region were found to be slightly too large and were somewhat reduced. Also, an upper bound on maximum allowable shift was used based on a 15-caliber body length. In other words, if a 20-caliber body were being considered, the maximum allowable shift in the center of pressure is based on a 15-caliber body. The final tabulation of shifts in the body-alone center of pressure as a function of AOA and Mach number is given in Table 1 of Ref. 3.

The other modification in the body-alone solution has to do with adding compressibility effects into the laminar skin-friction drag calculation. The laminar portion of the flow is based on

incompressible flow over a flat plate. The mean skin-friction coefficient is given by

$$C_{F_\ell} = 1.328/Re \tag{4}$$

A more accurate approach is to take into account compressibility for higher Mach number, higher altitude flight where a large portion of the boundary layer is laminar. Assuming a Prandtl number of 1.0, ratio of specific heats of 1.4, and exponent in the Sutherland viscosity law of 0.8, an improved formula can be derived based on Fig. 15.7 from Ref. 13. The mean skin-friction coefficient for laminar compressible boundary layers then becomes

$$C_{F_\ell} = (1/Re_\infty)\left[1.328 - 0.0236M_\infty - 0.00335M_\infty^2 + 0.000349M_\infty^3 - 8.54 \times 10^{-6}M_\infty^4\right] \tag{5}$$

The skin-friction drag is simply the mean skin-friction coefficient multiplied by the ratio of wetted area to reference area, i.e.,

$$C_{A_F} = C_{F_\ell}\frac{(A_{\text{wetted}})_\ell}{A_{\text{ref}}} + C_{F_T}\frac{(A_{\text{wetted}})_T}{A_{\text{ref}}} \tag{6}$$

Equation (5) will reduce the laminar-skin friction drag over the incompressible case. The higher the Mach number is, the greater the reduction.

Wing-Alone Improvements

A brief summary of the new wing-alone methodology[2] will be presented here for completeness. In essence, several alternative fourth-order methods for computing wing-alone lift were investigated.[2] The AP93[1] methodology used a second-order method. Above AOA of 25–30 deg, however, this second-order technique began to degrade in accuracy, and higher order methods were required. The new higher-order method is defined by

$$C_{N_W} = a_0 + a_1\alpha_W + a_2\alpha_W^2 + a_3\alpha_W^3 + a_4\alpha_W^4 \tag{7}$$

where $\alpha_W = |\alpha + \delta|$.

The constants a_i in Eq. (7) were defined based on five independent conditions and using data from Refs. 5, 9, and 12. The method allowed wing-alone aerodynamics to be calculated to AOA 180 deg. Since it has been well documented[2,3] and presented externally as well, no further discussion of the wing-alone methodology used in the AP95 will be given.

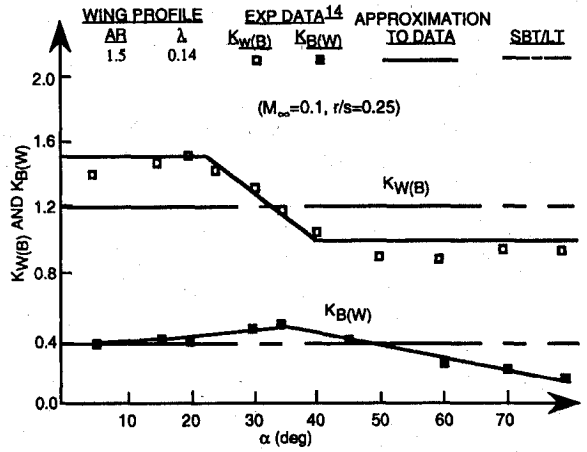

Fig. 2a Wing–body and body–wing interference lift factors.

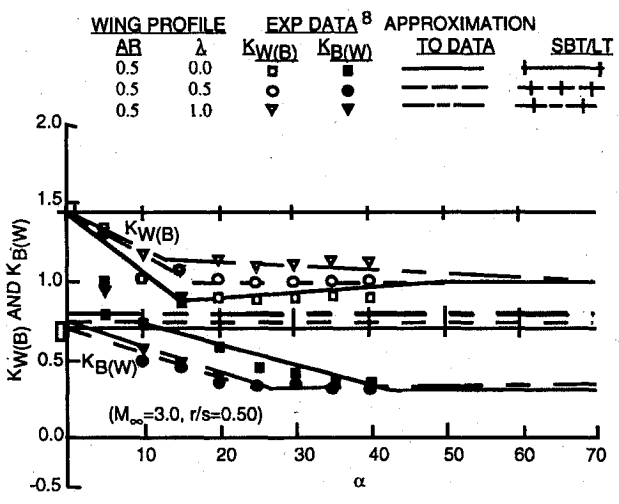

Fig. 2b Wing–body and body–wing interference factors.

Interference and Downwash Force and Center of Pressure

Referring to Eq. (1) and the discussion that follows, there are several interference factor terms that need to be defined. The approach used in the AP95 is similar to that used in the AP93 except more empirical constants are used as a result of the requirements for AOA greater than 30 deg. The databases used in the semiempirical model are those of Refs. 8, 9, 12, and 14. Examples of the interference factors for zero control deflection as a function of AOA are given in Figs. 2a and 2b. Figures 2a and 2b were derived from Refs. 14 and 8 data, respectively, with the wing-alone data determined from Refs. 5, 9, and 12. Reference 3 gives additional plots of data for Mach numbers 0.6, 0.8, 1.2, 1.5, 2.0, 2.5, 3.5, and 4.5 and for various aspect ratios and taper ratios. Note that Fig. 2b gives data only to AOA = 40 deg, whereas Fig. 2a has data to AOA = 80 deg.

In general, it was found that the interference factors $K_{W(B)}$ and $K_{B(W)}$ (or $K_{T(B)}$ and $K_{B(T)}$) could be placed in a general format shown in Figs. 3a and 3b. The empirical constants shown in the figures are defined in several tables in Ref. 3 as a function of Mach number and fin aspect and taper ratios. Note that the mathematical model for both $K_{W(B)}$ and $K_{B(W)}$ shown in Figs. 3a and 3b is defined by slender-body or linear theory plus deviations as AOA, Mach number, taper ratio, or aspect ratio changes.

In examining the nonlinear models for $K_{W(B)}$ and $K_{B(W)}$, it is instructive to try to correlate the mathematical models with the physics of the flow. The wing–body interference factor is somewhat easier to understand than the body–wing interference. The wing–body experimental data show that at low Mach number, slender-body theory

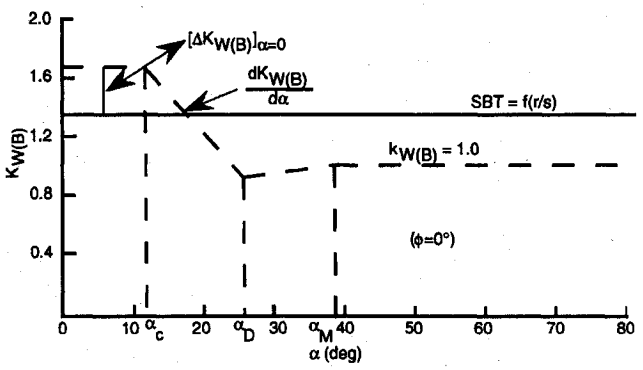

Fig. 3a Generic representation of $K_{W(B)}$: $K_{W(B)} = [K_{W(B)}]_{SBT} + f([\Delta K_{W(B)}]_{\alpha=0}, \alpha_c, [dK_{W(B)}/d\alpha], \alpha_D$, and $\alpha_M)$.

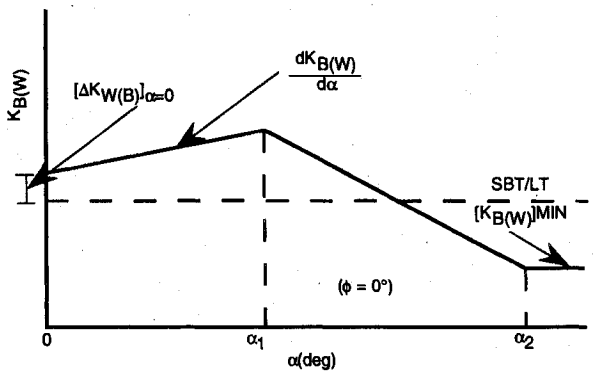

Fig. 3b Generic representation of $K_{B(W)}$. Parameters: $K_{B(W)} = [K_{B(W)}]_{LT_{SBT}} + f([\Delta K_{B(W)}]_{\alpha=0}, \alpha_1, \alpha_2, [dk_{B(W)}/d\alpha]$, and $[K_{B(W)}]_{MIN})$.

MACH	NONLINEAR MODEL
M≤0.8	If $\lvert\alpha_w\rvert \le 4.0 \rightarrow k_{W(B)} = 1.4[k_{W(B)}]_{SB}$ If $\lvert\alpha_w\rvert > 24.0 \rightarrow k_{W(B)} = 1.4[0.000794\lvert\alpha_w\rvert^2 - 0.0933\lvert\alpha_w\rvert + 2.71]$ $F = 1.1$
M=1.1	If $\lvert\alpha_w\rvert \le 15.0 \rightarrow k_{W(B)} = 1.3[k_{W(B)}]_{SB}$ If $\lvert\alpha_w\rvert > 15.0 \rightarrow k_{W(B)} = 1.3[0.00087\lvert\alpha_w\rvert^2 - 0.0825\lvert\alpha_w\rvert + 1.98]$ $F = 1.1$
M=1.5	If $\lvert\alpha_w\rvert \le 10.0 \rightarrow k_{W(B)} = 1.0[k_{W(B)}]_{SB}$ If $\lvert\alpha_w\rvert > 10.0 \rightarrow k_{W(B)} = 1.0[k_{W(B)}]_{SB} - 0.005[\lvert\alpha_w\rvert - 10.0]$ If $\lvert\alpha_w\rvert \le 20.0 \rightarrow F = 0.8$ If $\lvert\alpha_w\rvert > 20.0 \rightarrow F = 0.8 + 0.10[\lvert\alpha_w\rvert - 20.0]$
M=2.0	If $\lvert\alpha_w\rvert \le 10.0 \rightarrow k_{W(B)} = 0.9[k_{W(B)}]_{SB}$ If $\lvert\alpha_w\rvert > 10.0 \rightarrow k_{W(B)} = 0.9[k_{W(B)}]_{SB} - 0.003[\lvert\alpha_w\rvert - 10.0]$ If $\lvert\alpha_w\rvert \le 20.0 \rightarrow F = 0.8$ If $\lvert\alpha_w\rvert > 20.0 \rightarrow F = 0.8 + 0.17[\lvert\alpha_w\rvert - 20.0]$
M=2.3	If $\lvert\alpha_w\rvert \le 40.0 \rightarrow k_{W(B)} = 0.9[k_{W(B)}]_{SB}$ If $\lvert\alpha_w\rvert > 40.0 \rightarrow k_{W(B)} = 0.9[k_{W(B)}]_{SB} + 0.005[\lvert\alpha_w\rvert - 40.0]$ If $\lvert\alpha_w\rvert \le 30.0 \rightarrow F = 0.9$ If $\lvert\alpha_w\rvert > 30.0 \rightarrow F = 0.9 + 0.15[\lvert\alpha_w\rvert - 30.0]$
M=2.9	If $\lvert\alpha_w\rvert \le 40.0 \rightarrow k_{W(B)} = 0.9[k_{W(B)}]_{SB}$ If $\lvert\alpha_w\rvert > 40.0 \rightarrow k_{W(B)} = 0.9[k_{W(B)}]_{SB} + 0.005[\lvert\alpha_w\rvert - 40.0]$ If $\lvert\alpha_w\rvert \le 30.0 \rightarrow F = 0.9$ If $\lvert\alpha_w\rvert > 30.0 \rightarrow F = 0.9 + 0.17[\lvert\alpha_w\rvert - 30.0]$
M=4.0	If $\lvert\alpha_w\rvert \le 20.0 \rightarrow k_{W(B)} = 0.8[k_{W(B)}]_{SB}$ If $\lvert\alpha_w\rvert > 20.0 \rightarrow k_{W(B)} = 0.8[k_{W(B)}]_{SB} + 0.007[\lvert\alpha_w\rvert - 20.0]$ If $\lvert\alpha_w\rvert \le 30.0 \rightarrow F = 0.9$ If $\lvert\alpha_w\rvert > 30.0 \rightarrow F = 0.9 + 0.2[\lvert\alpha_w\rvert - 30.0]$
M≥4.6	If $\lvert\alpha_w\rvert \le 20.0 \rightarrow k_{W(B)} = 0.75[k_{W(B)}]_{SB}$ If $\lvert\alpha_w\rvert > 20.0 \rightarrow k_{W(B)} = 0.75[k_{W(B)}]_{SB} + 0.013[\lvert\alpha_w\rvert - 20.0]$ If $\lvert\alpha_w\rvert \le 35.0 \rightarrow F = 0.9$ If $\lvert\alpha_w\rvert > 35.0 \rightarrow F = 0.9 + 0.2[\lvert\alpha_w\rvert - 35.0]$
Where $\alpha_w = \alpha + \alpha$ and $k_{B(W)} = [k_{B(W)}]_{SB}$	

Fig. 4 Nonlinear wing–body interference model for control deflection.

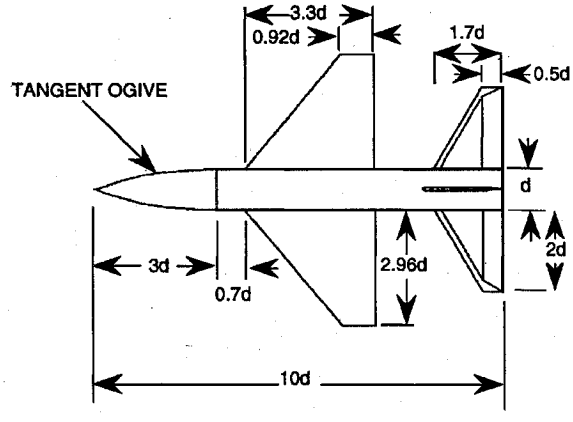

Fig. 5a Wing–body–tail configuration used for comparing AP95 to experiment[11] and AP93: $(AR)_T = 3.64$, $\lambda_T = 0.29$, $d = 2.6$ in., $(AR)_W = 2.81$, and $\lambda_W = 0.28$.

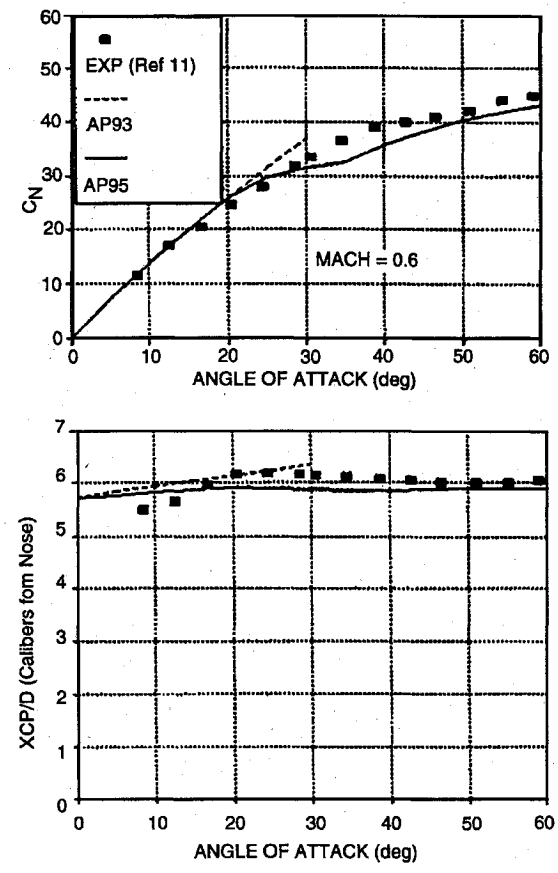

Fig. 5b Normal force coefficient and center of pressure comparisons at $M_\infty = 0.6$.

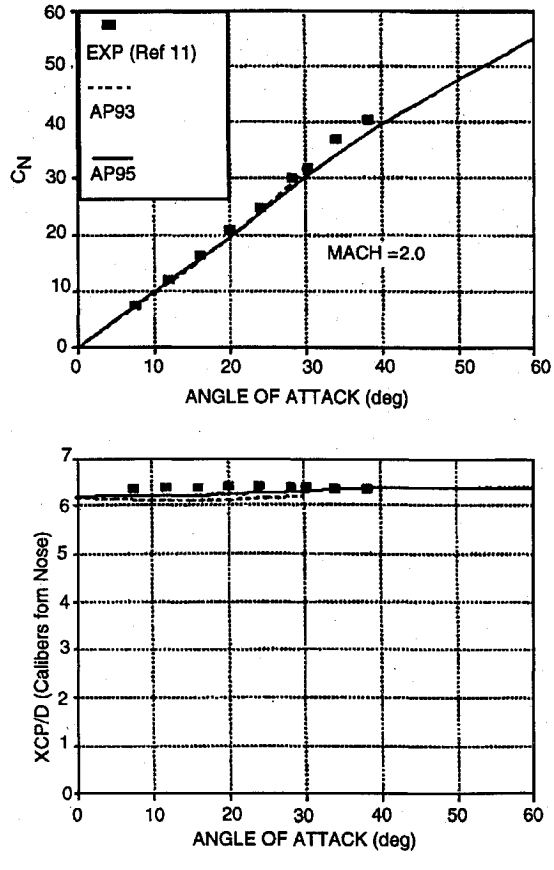

Fig. 5c Normal force coefficient and center of pressure comparisons at $M_\infty = 2.0$.

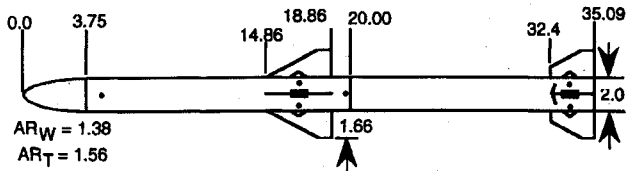

Fig. 6a MMPT configuration tested at $M = 0.2$ (Ref. 15).

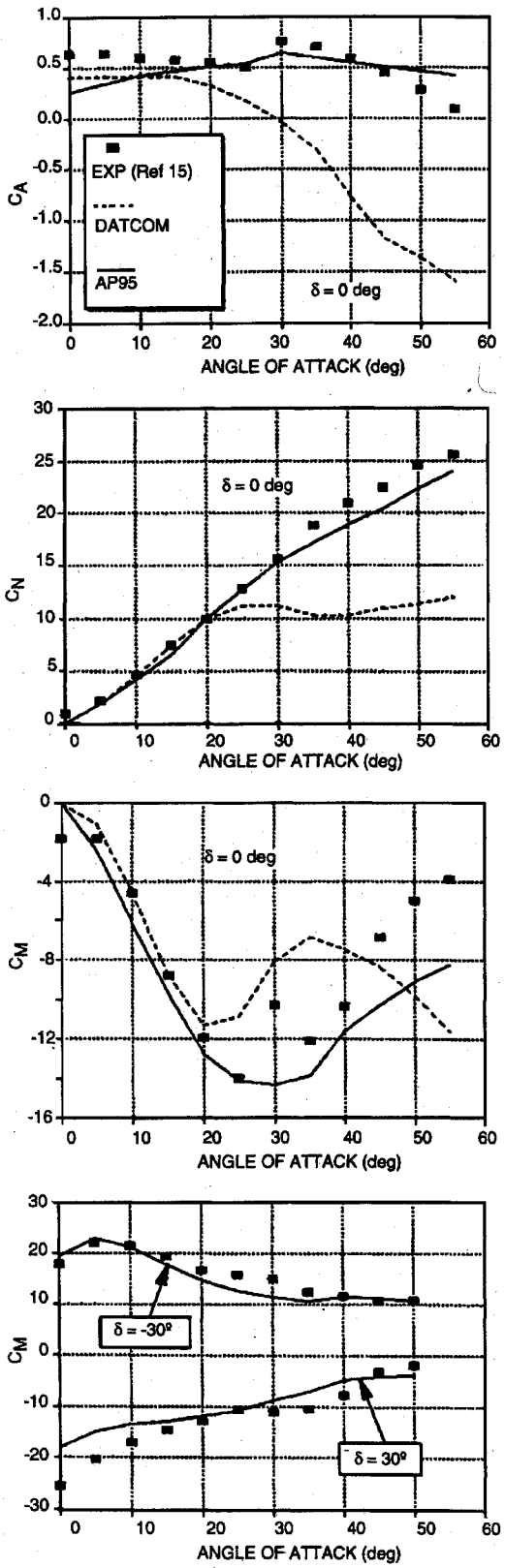

Fig. 6b Comparisons of experimental and predicted static aerodynamic coefficients.

slightly underpredicts the experimental data. As AOA is increased, $K_{W(B)}$ starts decreasing and in some cases decreases below its wing-alone value. As AOA increases, $K_{W(B)}$ approaches its wing-alone value. As Mach number increases, the positive interference lift on the wing, caused by the presence of the body, is lost faster and faster as AOA increases. That is, the wing-alone solution is recovered much faster at high Mach number, as AOA increases, than at low Mach number. This rapid decrease of $K_{W(B)}$ to one at higher Mach numbers is believed to be the result of the Newtonian impact mechanism where, at high Mach number, the momentum of the air particle is lost almost entirely upon direct impact on a surface, as opposed to wrapping around the surface and carrying some of the momentum with it, as at low Mach numbers.

The $K_{B(W)}$ model contains body vortex effects, nose- and wing-to-wing shock effects, as well as the usual added dynamic pressure of the body caused by the presence of the wing. The present direct approach of modeling these effects simultaneously neglects some of the scale effects caused by the position of the wing on the body. The alternative to this approach is to attempt to estimate each of the physical effects analytically, subtract them out of the data, and then add them back in using the same analytical approach but for a different configuration.[5]

In general, $K_{B(W)}$ actually increases with AOA at low Mach numbers to a certain point, where it starts decreasing analogous to $K_{W(B)}$. However, a certain amount of lift or force enhancement is gained all of the way to $\alpha = 90$ deg for low Mach numbers, as shown in Fig. 2a. This phenomenon is assumed to occur all of the way to $M = 6.0$ based on extrapolated data from the point where experimental data end.[3]

Additional higher AOA data above $\alpha = 40$ deg is needed for both $K_{W(B)}$ and $K_{B(W)}$ to modify the assumed extrapolations of the models for $K_{W(B)}$ and $K_{B(W)}$ at high AOA. Until additional data are available, however, the approximate nonlinear models for $K_{W(B)}$ and $K_{B(W)}$ can be used to estimate aerodynamics for engineering use. This statement will be validated for a limited set of flight conditions in a later section.

The center of pressure of the carryover interference force on the wing is assumed to lie at the wing-alone center of pressure as defined in Ref. 1. The center of pressure of the interference force on the body is assumed to occur at the same point as computed by linear theory or slender-body theory (dependent on Mach number and aspect ratio primarily), also as done in Ref. 1.

The other three terms of Eq. (1), as yet not discussed, are $k_{W(B)}$, $k_{B(W)}$, and $C_{N_{T(V)}}$. The mathematical model used in AP95 is the same as in AP93, except the empirical constants have been adjusted because of the higher AOA and because r/s has been eliminated from the nonlinear terms of $K_{W(B)}$ and $K_{B(W)}$. This model for the as yet undefined terms of Eq. (1) is

$$k_{W(B)} = C_1(M)\left[k_{W(B)}\right]_{\text{SBT}} + C_2(|\alpha_W|, M) \tag{8}$$

$$k_{B(W)} = \left[K_{W(B)} - k_{W(B)}\right]_{\text{SBT}} \tag{9}$$

$$C_{N_{T(V)}} = \frac{\left(C_{N_\alpha}\right)_W \left(C_{N_\alpha}\right)_T \left[K_{W(B)} \sin\alpha + F k_{W(B)} \sin\delta_W\right] i (s_T - r_T) A_W}{2\Pi (AR)_T (f_W - r_W) A_{\text{ref}}} \tag{10}$$

where $F = C_3(M, |\alpha_W|)$.

The updated constants C_1, C_2, and C_3 are all defined in Fig. 4. Note that all of the nonlinearities for the interference factors resulting from control deflection have been included in the $k_{W(B)}$ term, and $k_{B(W)}$ is still defined by slender-body theory. This definition is because the constants C_1, C_2, and C_3 were determined through numerical experimentation and there was no way to separate the nonlinear effects between the two terms. Also note that the $C_{N_{T(V)}}$ term is identical to linearized theory[10] except for the factor F, which is used here to account for the stronger nonlinearities associated with control deflection. However, all of the terms in Eq. (10) are in themselves nonlinear as opposed to the linear counterparts.[10]

Nonlinearities Not Modeled Completely

Several aerodynamic nonlinearities are either not modeled or only partially modeled. These include asymmetrically shed body vortices

(which can be important primarily for $M \leq 2.0$ and $\alpha > 25$ deg), internal shock interactions, and cross coupling of the aerodynamics resulting from roll. The asymmetric vortices are only modeled partially in the sense that some account of the forward shift in body-alone center of pressure is predicted based on a large database. Internal shock interactions between a forward- and aft-mounted set of fins are not modeled at all. Shock interactions between the bow shock and the most forward-mounted set of fins are partially included. Finally, no account of cross coupling of aerodynamics between pitch and roll is attempted as this is an extremely difficult task for a semiempirical code. More detailed discussion of these nonlinearities is given in Ref. 3.

Results and Discussion

Three example cases will be considered for validation of the new technology. These example cases were outside the database on which the AP95 methodology was developed. Several other examples are given in Ref. 3.

The first case is a wing–body–tail case[11] (see Fig. 5a). This case was also considered for AP93, but only up to 30-deg AOA, since that was the limit of that technology. The normal force coefficient and center-of-pressure comparisons of the AP95, AP93, and data[11] are shown in Figs. 5b and 5c.

In general, the AP95 gives quite acceptable results for an engineering code for this configuration compared to data at both Mach numbers considered. A slight discontinuity is apparent in the slope of the C_N curve at $\alpha = 35$ deg and $M_\infty = 0.6$. This slight discontinuity is caused by the fact that at subsonic Mach numbers, the wing basically stalls around AOA of 25–40 deg. The wing-alone method of the AP95 blends this discontinuous behavior out, and the fourth-order method for the wing tends to show a discontinuous slope of the C_N curve at low Mach number. If the configuration of Fig. 5a were body dominated, this behavior would not be as obvious, but since it is wing dominated, the wing behavior is more prevalent.

The second case is more missilelike compared to Fig. 5a. This case is a wing–body–tail configuration (see Fig. 6a) tested at low Mach number ($M = 0.2$) in the U.S. Naval Postgraduate School wind tunnel in Monterey, California.[15] Axial, normal, and pitching moment coefficients are shown in Fig. 6b as a function of AOA and tail control deflection. Results are given for the AP95 and data and missile DATCOM[6] results from Ref. 15. These results for AP95 compared to data are very encouraging for all of the coefficients, as it appears the nonlinearities are being modeled reasonably well. The axial force is not as accurate as desired but the authors state[15]

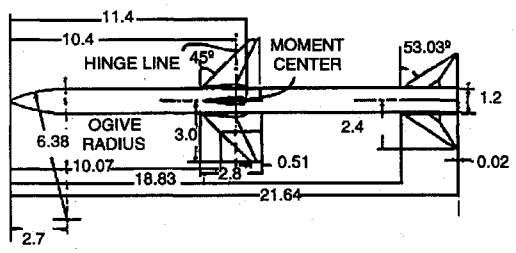

Fig. 7a Air-to-air missile configuration used in validation process.[16,17]

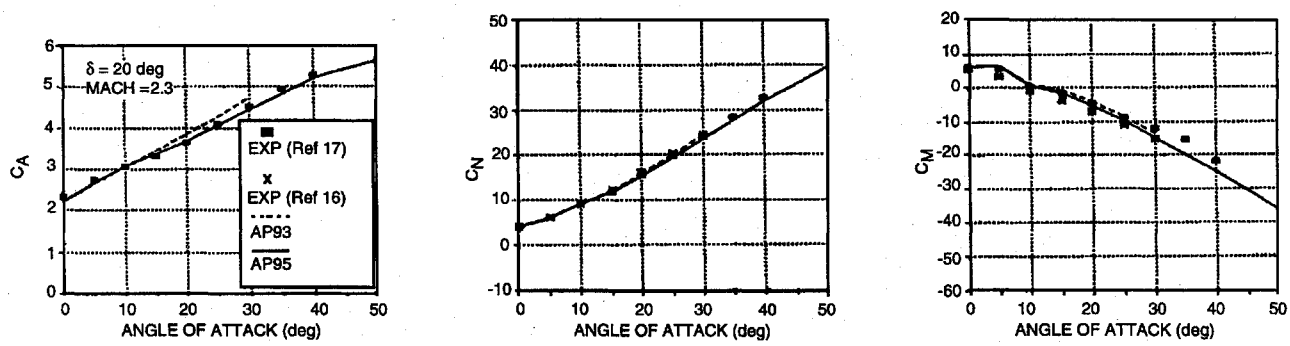

Fig. 7b Static aerodynamic coefficient comparisons.

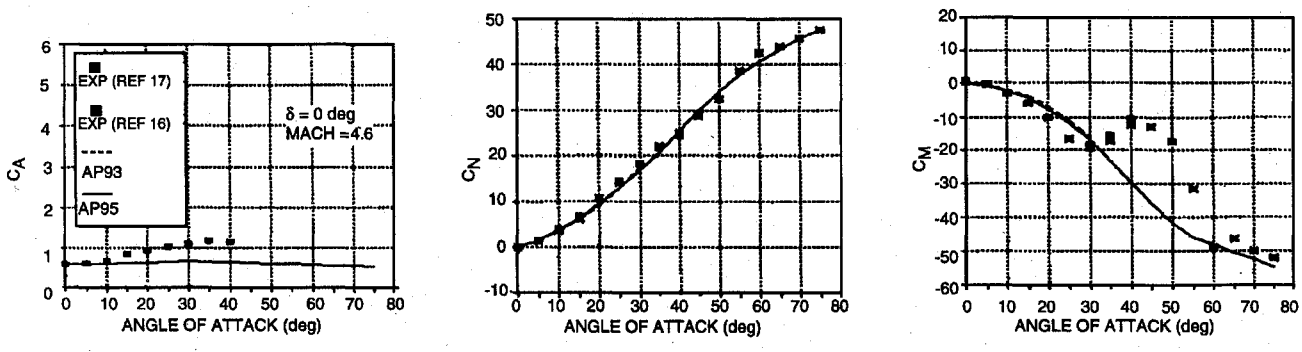

Fig. 7c Static aerodynamic coefficient comparisons for Fig. 7a configuration, $M_\infty = 4.6$.

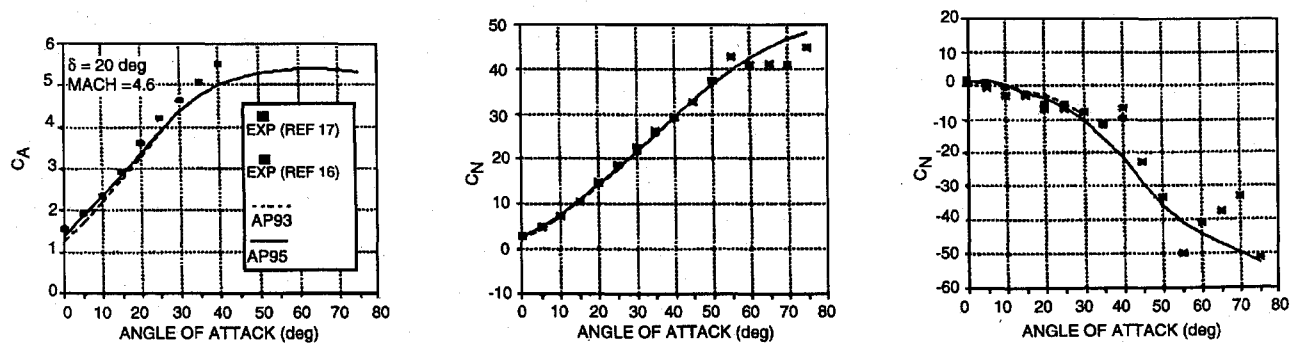

Fig. 7d Static aerodynamic coefficient comparisons for Fig. 7a configuration, $M_\infty = 4.6$.

the sting was designed for normal vs axial force; the discrepancies are reasonable on that basis. The pitching moment comparisons for control deflection of ±30 deg shown in Fig. 6b are quite gratifying because these curves utilize all of the new technology developed at this low Mach number.

The final validation case considered is a version of the Seasparrow missile that has an extensive supersonic wind-tunnel database including AOA to 70 deg at some Mach numbers, and with control deflections to ±20 deg. The first database includes AOA to 70 deg at Mach numbers of 2.3 and 4.6 only.[16] This configuration was tested with wiring tunnels on the exterior of the missile, which contributed somewhat to the aerodynamics. The other database is more extensive in Mach number in that Mach numbers of 1.5, 2.0, 2.35, 2.87, 3.95, and 4.63 were tested, but AOA was limited to 45 deg (Ref. 17). In the comparisons, the data at $M = 2.3$ and 2.35 and at $M = 4.6$ with and without wiring tunnels will be shown on the same figures. Reference 3 gives all Mach number results.

Figure 7a shows the external view of the configuration tested without the wiring tunnels.[17] The configuration is 18 calibers in length with a 2.25-caliber tangent ogive nose. It has wings with aspect ratio of 2.8 and tail surfaces of aspect ratio 2.6. The wings are used for control, and the pitching moments are referenced to a point 8.66 calibers from the nose tip.

Figures 7b–7d present the C_A and C_N comparisons of the AP95 with all data available at $M = 2.3, 2.35$, and 4.6. The data that extend to AOA = 70 deg have wiring tunnels present, whereas the data without wiring tunnels only go to 45-deg AOA. Note again that good agreement between the AP95 and data is obtained for most values of α and δ.

Pitching moments in Fig. 7b are also predicted fairly well at $M = 2.3$ for all AOA, because the internal shock interactions are not as severe. However, at Mach 4.6 (see Figs. 7c and 7d), the internal shock interactions are very severe, and the AP95 does not predict the nonlinearities that occur between AOA of 30 and 60 deg. However, pitching moments are predicted quite well for AOA less than 30 deg and greater than 60 deg. These internal shock interactions are believed to be the cause of the axial force underprediction at $M = 4.6$ and $\alpha > 15$ deg as well.

In trying to understand the phenomena occurring in Figs. 7c and 7d, the study of Ref. 18 was examined. This work involved wind-tunnel tests conducted at Mach number 2.7 on a wing–body configuration similar to the configuration in Fig. 7a without the tail surfaces. Body and wing pressure measurements, oil flow measurements, and schlieren photographs were taken. The data showed that, even at a moderate supersonic Mach number of 2.7, the bow shock intersected the wing in the windward plane at AOA of 30 deg, approximately. When this occurred, a trailing shock was created behind the wing. Of course, if a tail surface were present, this trailing shock would have the potential to interact with the tail surface. As Mach number increases, this trailing shock increases in strength, causing a much stronger impact on the tail surface. Since the tail surface is over 7 calibers from the moment center, a small change in tail-normal force has a much larger impact on the pitching moment. The other physical phenomenon indicated was a fairly strong change in the pressure distribution of the carryover lift on the body.[18] Most likely, the center of pressure of this carryover lift also is affected, which also will change the pitching moment.

Conclusions

The work presented was directed at developing an engineering version of an APC for AOA > 30 with acceptable accuracy. This new code could then be used to meet all operational requirements for the roll position of $\Phi = 0$ deg (fins in plus fin orientation). The following conclusions and recommendations are made.

1) Based on limited comparisons to date, the average accuracy levels of ±10% on C_A and C_N and ±4%ℓ have been maintained for the AP95 except in regions of strong shock interactions (high Mach number, high AOA). Average accuracy means the average of the accuracy of the AP95 compared to experimental data for several AOAs and Mach numbers.

2) Many extrapolations of data and engineering judgement were required in development of the nonlinear semiempirical methodology. Additional wind tunnel–data or full Navier–Stokes computations or both could eliminate some of these assumptions and improve on the existing methodology. Particular needs are the effect of r/s on $K_{B(W)}$ for all Mach numbers and at the AOA > 5 deg. Any new tests should be done with a large wing planform mounted in the middle of the body and with various values of r/s, α, and M.

Acknowledgments

Appreciation is expressed to Tom Loftus, Craig Porter, Robin Staton, and Gil Graff, who manage the technology programs that supported this task, and to Dave Siegel, who sponsored the work.

References

[1]Moore, F. G., Hymer, T. C., and McInville, R. M., "A Planar Nonlinear Missile Aeroprediction Code for all Mach Numbers," AIAA Paper 94-0026, Jan. 1994.

[2]Moore, F. G., and McInville, R. M., "A New Method for Calculating Wing Alone Aerodynamics to Angle of Attack 180°," U.S. Naval Surface Warfare Center, NSWCDD/TR-94/3, Dahlgren, VA, March 1994.

[3]Moore, F. G., McInville, R. M., and Hymer, T., "The 1995 Version of the NSWC Aeroprediction Code: Part I—Summary of New Theoretical Methodology," U.S. Naval Surface Warfare Center, NSWCDD/TR-94/379, Dahlgren, VA, Feb. 1995.

[4]Devan, L., Mason, L., and Moore, F. G., "Aerodynamics of Tactical Weapons to Mach Number 8 and Angle of Attack 180°," AIAA Paper 82-0250, Jan. 1982.

[5]Nielsen, J. N., Hemsch, M. H., and Smith, C. A., "A Preliminary Method for Calculating the Aerodynamic Characteristics of Cruciform Missiles to High Angles of Attack Including Effects of Roll Angle and Control Deflections," U.S. Office of Naval Research, Rept. ONR-CR215, 216, 4F, Arlington, VA, Nov. 1977.

[6]Vukelich, S. R., and Jenkins, J. E., "Missile DATCOM: Aerodynamic Prediction on Conventional Missiles Using Component Build-Up Techniques," AIAA Paper 84-0388, Jan. 1984.

[7]Ericsson, L. E., and Reding, J. P., "Asymmetric Vortex Shedding from Bodies of Revolution," *Tactical Missile Aerodynamics*, edited by M. J. Hemsch and J. N. Nielsen, Vol. 104, Progress in Astronautics and Aeronautics, AIAA, New York, 1986, Chap. 7, pp. 243–296.

[8]Anon., "NASA Langley Research Center Tri-Service Missile Data Base," Transmitted from NASA/LRC Jerry M. Allen to NSWCDD, U.S. Naval Surface Weapons Center, Dahlgren Div., Dahlgren, VA, Nov. 1991 (formal documentation of database process).

[9]Stallings, R. L., Jr., and Lamb, M., "Wing-Alone Aerodynamic Characteristics for High Angles of Attack at Supersonic Speeds," NASA TP 1989, July 1981.

[10]Pitts, W. C., Nielsen, J. N., and Kaatari, G. E., "Lift and Center of Pressure of Wing–Body–Tail Combinations at Subsonic, Transonic, and Supersonic Speeds," NACA TR 1307, 1957.

[11]Jorgenson, L. H., "Predictions of Static Aerodynamic Characteristics for Slender Bodies Alone and with Lifting Surfaces to Very High Angles of Attack," NASA TR R-474, Sept. 1977.

[12]Baker, W. B., Jr., "Static Aerodynamic Characteristics of a Series of Generalized Slender Bodies With and Without Fins at Mach Numbers from 0.6 to 3.0 and Angles of Attack from 0 to 180°," Arnold Engineering and Development Center, AEDC-TR-75-124, Vols. 1 and 2, Tullahoma, TN, May 1976.

[13]Schlichting, H., *Boundary Layer Theory*, 4th ed., McGraw–Hill, New York, p. 348.

[14]Meyer, J., "Effects of the Roll Angle on Cruciform Wing–Body Configurations at High Incidences," *Journal of Spacecraft and Rockets*, Vol. 31, No. 1, 1994, pp. 113–122.

[15]Smith, E. H., Salazar, M. E., Hebbar, S. K., and Platzer, M., "Aerodynamic Characteristics of the MMPT ATD Vehicle at High Angles of Attack," AIAA Paper 93-3493, Aug. 1993.

[16]McKinney, R. L., "Longitudinal Stability and Control Characteristics of an Air-to-Air Missile Configuration at Mach Numbers of 2.3 and 4.6 and Angles of Attack from −45, to 90°," NASA TMX-846, 1972.

[17]Monta, W. J., "Supersonic Aerodynamic Characteristics of a Sparrow III Type Missile Model with Wing Controls and Comparison with Existing Tail-Control Results," NASA TP 1078, Nov. 1977.

[18]Agnone, A. M., Zakkay, V., and Tory, E., "Aerodynamics of Slender Finned Bodies at Large Angles of Attack," AIAA Paper 77-666, June 1977.

R. M. Cummings
Associate Editor